Investigations on macro-element modelling of bucket foundations for offshore wind turbines

Foglia, Aligi; Govoni, Laura; Gottardi, Guido; Ibsen, Lars Bo

Publication date:
2014

Document Version
Publisher's PDF, also known as Version of record

Investigations on macro-element modelling of bucket foundations for offshore wind turbines

Aligi Foglia
Laura Govoni
Guido Gottardi
Lars Bo Ibsen

ISSN 1901-7278
DCE Technical Memorandum No. 48

DEPARTMENT OF CIVIL ENGINEERING
AALBORG UNIVERSITY

Aalborg University
Department of Civil Engineering
Division of Structures, Materials and Geotechnics

DCE Technical Memorandum No. 48

Investigations on macro-element modelling of bucket foundations for offshore wind turbines

by

Aligi Foglia
Laura Govoni
Guido Gottardi
Lars Bo Ibsen

September 2014

Scientific Publications at the Department of Civil Engineering

Technical Reports are published for timely dissemination of research results and scientific work carried out at the Department of Civil Engineering (DCE) at Aalborg University. This medium allows publication of more detailed explanations and results than typically allowed in scientific journals.

Technical Memoranda are produced to enable the preliminary dissemination of scientific work by the personnel of the DCE where such release is deemed to be appropriate. Documents of this kind may be incomplete or temporary versions of papers—or part of continuing work. This should be kept in mind when references are given to publications of this kind.

Contract Reports are produced to report scientific work carried out under contract. Publications of this kind contain confidential matter and are reserved for the sponsors and the DCE. Therefore, Contract Reports are generally not available for public circulation.

Lecture Notes contain material produced by the lecturers at the DCE for educational purposes. This may be scientific notes, lecture books, example problems or manuals for laboratory work, or computer programs developed at the DCE.

Theses are monograms or collections of papers published to report the scientific work carried out at the DCE to obtain a degree as either PhD or Doctor of Technology. The thesis is publicly available after the defence of the degree.

Latest News is published to enable rapid communication of information about scientific work carried out at the DCE. This includes the status of research projects, developments in the laboratories, information about collaborative work and recent research results.

Published 2014 by
Aalborg University
Department of Civil Engineering
Sofiendalsvej 9-11,
DK-9200 Aalborg SV, Denmark

Printed in Aalborg at Aalborg University

ISSN 1901-7278
DCE Technical Memorandum No. 48

Investigations on macro-element modelling of bucket foundations for offshore wind turbines

Aligi Foglia[1], Laura Govoni[2], Guido Gottardi[2], Lars Bo Ibsen[1]

[1]Department of Civil Engineering, Aalborg University
[2]DICAM, University of Bologna

In this report a macro-element model for bucket foundations is formulated and validated against small-scale experimental results. The topics investigated are the response of the foundation under general monotonic loading and the long-term accumulated displacements under cyclic loading. The macro-model for shallow foundations proposed by Nova and Montrasio (1991) is modified to comply with the response of skirted foundations for offshore wind turbines under general loading. On the base of di Prisco et al. (2003a), the constitutive relationship is modified to account for cyclic loading. The validation of the macro-model against the physical experiments shows promising results.

1 Introduction

Offshore wind turbines (OWTs) are light and dynamically sensitive structures. This determines a unique loading condition which consists of large cyclic overturning moment M, relatively large cyclic horizontal load H and small vertical load V. The design of these structures is mostly driven by the dynamic properties of the system and by the long-term response under cyclic loading in terms of stiffness and accumulated displacements (Haigh, 2014). This report deals with

the substantially drained response of bucket foundations under monotonic and cyclic loading. More specifically, a macro-model to evaluate the response of bucket foundations supporting OWTs, is formulated. This chapter includes a literature review and a description of the contribution of the paper. The chapter "Physical modelling" presents the experiments used to calibrate the parameters of the model. The chapter "Analytical modelling" describes the analytical models used and shows comparisons with the experimental results.

1.1 Literature review

Through macro-element modelling, preliminary estimations of the response of a geotechnical system can be obtained. This technique is applicable to many kinds of geotechnical problems but its primary and best-known application is on shallow foundations. In Wood (2012) three different applications of macro-element modelling are thoroughly described. Generally speaking, a macro-model consists of three elements: geotechnical structure, surrounding soil and displacement or load field applied to the system, *cf.* Figure 1. For shallow foundations, the concept has perhaps its origin with Roscoe and Schofield (1956). During the last decades, the theory of plasticity has been employed by a number of researchers to investigate the response of shallow foundations under general loading. The main objective of these studies has been to overcome the traditional semi-empirical method to calculate the bearing capacity in favor of a new approach capable of capturing the non-linearity of the problem and suitable for numerical simulations. An early study on interaction diagrams is Butterfield and Ticof (1979). Subsequently, Nova and Montrasio (1991) derived a model for strip footing. Gottardi and Butterfield (1993, 1995) carried out important studies on shallow footings, addressing failure surfaces and displacement patterns under general planar loading. Martin (1994) conceived Model B for spudcans on clay. Gottardi et al. (1999) developed the basis for Model C (footings on sand) which was then completed by Houlsby and Cassidy (2002). Byrne and Houlsby (2001) extrap-

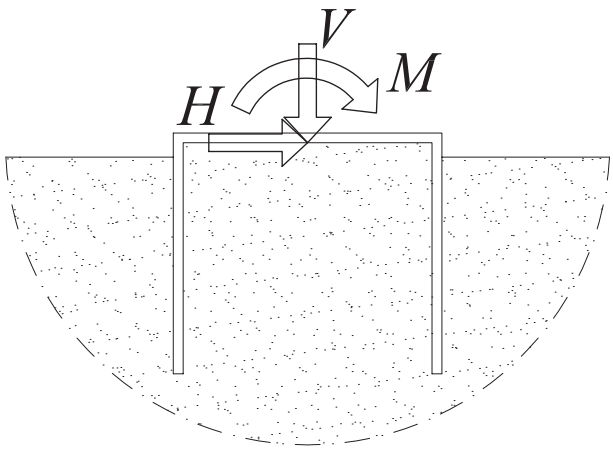

Figure 1: Fundamental macro-element components: foundation, surrounding soil and three-dimensional load field

olated the yielding surfaces for footings on carbonate sands. Bienen et al. (2006) explored the behaviour of footings in six degrees of freedom (6-DOF). To calibrate a macro-model, physical experiments are essential. Often, in order to extrapolate the necessary model parameters, loading paths that do not resemble possible real loading conditions must be carried out. 1g physical models have been by far used to obtain the model parameters. Recently, also centrifuge tests have been conducted on this purpose. To a large extend centrifuge data corroborated the findings of single gravity modelling (Govoni et al., 2011; Zhang et al., 2014).

Of current interest is cyclic macro-modelling. The majority of the studies on cyclic macro-modelling concerns structures under seismic excitations. In the last decade, many contributions have been given to this research topic. A comprehensive and very informative document on this theme is di Prisco (2012). Cremer et al. (2001) describe a macro-element formulation for a shallow foundation in plain strain. They suggest a multi-surface plasticity model and take into account the non-linearity of the material and the non-linearity due to the partial uplift of the footing. Chatzigogos et al. (2011) developed further the work of Cremer et al. (2001) and conceived a bounding surface hypoplastic model. Nguyen-Sy (2006) derived a hyperplastic model (Houlsby and Puzrin, 2007) and applied it to bucket foundations. di Prisco et al. (2003a,

2003b) integrated the Nova and Montrasio (1991) model with a boundary surface model to represent cyclic loading. An application of the latter is presented in di Prisco et al. (2006). Buscarnera et al. (2010) used the same model to calculate the accumulated displacement of onshore wind turbine on gravity based foundation under wind loading. Kafle and Wuttke (2013) slightly modified the model of Nova and Montrasio (1991) and di Prisco et al. (2003a) to predict the response of a footing on unsaturated soil. Salciarini and Tamagnini (2009) proposed a hypoplastic macrolement for surface footings. The same model was then expanded to 6-DOF in Tamagnini et al. (2013).

1.2 Outline of the study

The aim of this study is to show that experimental results of bucket foundations under monotonic and cyclic loading can be interpreted by means of a macro-element model. Prior to model the cyclic loading response, it is fundamental to have a reliable and consistent description of the monotonic behaviour. The model chosen for interpreting the monotonic experiments is the Nova and Montrasio (1991) model (NMM). This choice is driven by the possibility of modelling long-term cyclic loading as elucidated in di Prisco et al. (2003a, 2003b) and Buscarnera et al. (2010). In order to have satisfying match with the experimental data, the NMM is necessarily modified. A simplified version of the boundary surface model proposed by (di Prisco et al., 2003a) is incorporated into the modified NMM to model the cyclic loading response. The macro-model simulates satisfactorily the physical response. Particularly, the comparison with four experimental cyclic tests is encouraging and reveals that certain features of the cyclic behaviour can be replicated by the macro-model.

It should be said upfront that a rigorous extrapolation of the model parameters is beyond the scope of this work. Regardless, the results achieved are meaningful and clearly highlight the potential of the model.

2 Physical modelling

A large number of single gravity tests of bucket foundations were carried out at Aalborg University to explore the cyclic lateral response of the foundation in dense saturated sand (Foglia et al., 2014). Based on the experimental results, the empirical model predicting the long-term accumulated rotation proposed by LeBlanc et al. (2010) was calibrated for dense saturated sand and extended to three different embedment ratios, $d/D = 0.5$, $d/D = 0.75$ and $d/D = 1$ where d is the embedment length and D the diameter of the foundation. In this study a more sophisticated interpretation based on the macro-element philosophy is proposed. In this section a selected series of tests which are necessary to the model formulation is presented. Nine monotonic tests and four cyclic loading tests are chosen to extrapolate some of the model parameters and to validate the model. All the experiments are listed in Table 1 where M_{R} is the moment capacity and M_{max} and M_{min} are the maximum and the minimum moment applied in a cyclic loading test. Eight monotonic tests (S13, S19, S25, S26, S27, S28, S29 and S30) are constant V tests with five different $M/(HD)$ ratios. One monotonic test (S64) is a pure vertical loading test until failure. The cyclic loading tests are constant V tests with $M/(HD) = 1.987$. The three different loading paths are represented on the three two-dimensional load planes, $(M/D - V)$, $(M/D - H)$ and $(H - V)$, in Figure 2. The tests were conducted with two different rigs but with the same bucket foundation and on the same sand, Aalborg University Sand No. 1 (*cf.* Table 2 for the index properties of the sand). The bucket foundation tested is made of steel and has the following features: outer diameter, $D = 300$ mm, length of the skirt, $d = 300$ mm, wall thickness, $t = 1.5$ mm, lid thickness, $t_l = 11.5$ mm and self-weight, $W = 125$ N. The cyclic tests and all the monotonic tests except for S64, were conducted with the experimental rig described in detail in Foglia et al. (2014). The size of the sand sample is 1600 x 1600 x 1150 mm; a picture of the setup is shown in Figure 3.

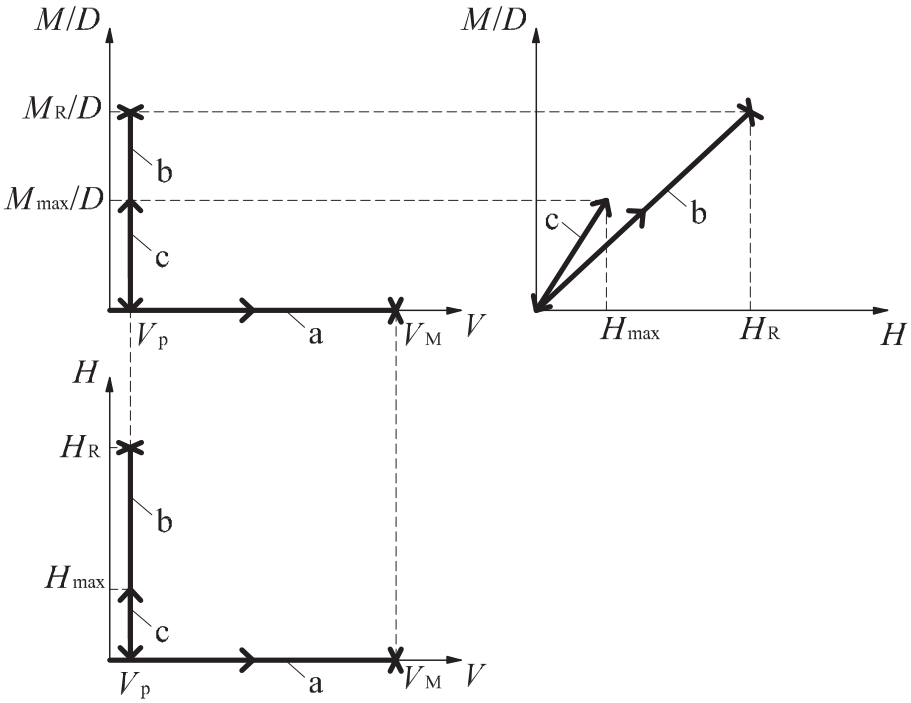

Figure 2: The three loading paths a, b and c on the three two-dimensional load planes: a) monotonic V test until failure; b) monotonic constant V test until failure, with constant $M/(HD)$; c) cyclic constant V test until failure, with constant $M/(HD)$

Table 1: Selected experimental tests for the model calibration and validation

Test name	$M/(HD)$ [-]	V [N]	M_{max}/M_R [-]	M_{min}/M_{max} [-]
S13	3.010	241	-	-
C16	1.987	241	0.403	-0.047
C18	1.987	241	0.299	-0.042
S19	1.987	241	-	-
C20	1.987	241	0.353	-0.595
S25	1.100	241	-	-
S26	5.820	241	-	-
S27	8.748	241	-	-
S28	5.819	241	-	-
S29	3.010	241	-	-
S30	1.987	241	-	-
S33	1.987	241	0.377	-0.316
S64	Pure vertical loading test			

Table 2: Index properties of Aalborg University sand No. 1

Property	Value	Unit
Grain diameter corresponding to 50% passing	0.14	[mm]
Uniformity coefficient	1.78	[-]
Specific grain density	2.64	[-]
Maximum void ratio	0.86	[-]
Minimum void ratio	0.55	[-]

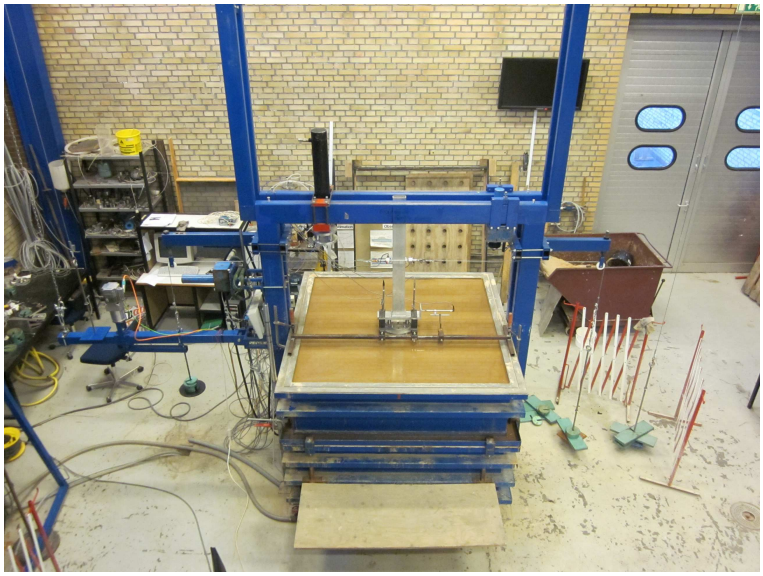

Figure 3: Picture of the experimental rig adopted to perform all the tests except for S64

The vertical load acting on the foundation during the tests includes the buoyant self-weight of the bucket and the weight of the measuring system mounted on the foundation. V is for each test equal to 241 N. The monotonic tests were displacement controlled tests until failure. One example of load-displacement curves for each $M/(HD)$ ratio is illustrated in Figure 4. The cyclic tests were load controlled with loading frequency $f_l = 0.1$ Hz and number of cycles $N = 5 \cdot 10^4$. Figures 5 and 6 depict the first 100 cycles of test C16.

A second testing rig, with a much more powerful actuator and a larger sand sample, was employed to run the pure vertical loading test until failure, test S64. This testing rig was designed to test bucket foundations with $D = 1000$ mm. A detailed description of the laboratory setup

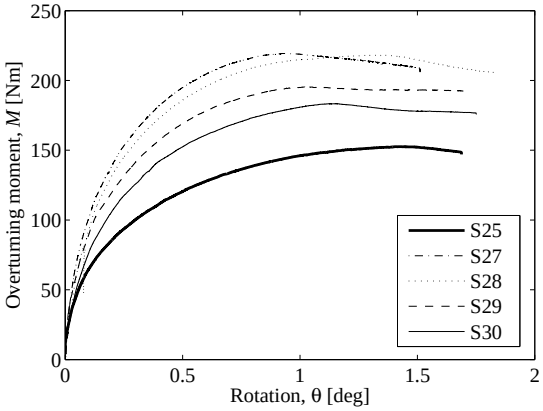

Figure 4: Example of monotonic tests, $M - \theta$ curves of 5 tests with different $M/(HD)$ ratio

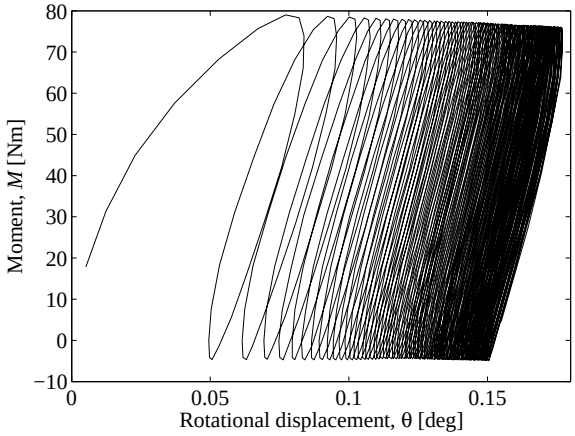

Figure 5: Experimental $M-\theta$ curve, test C16, first 100 cycles

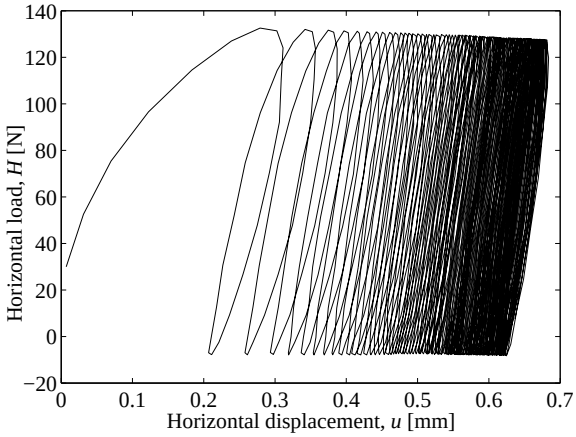

Figure 6: Experimental $H-u$ curve, test C16, first 100 cycles

is available in Vaitkunaite et al. (2014). In test S64, a local shear failure of the soil can be observed, *cf.* section 3.1.2.

The bearing capacity of the foundation is obtained as $V_{\mathrm{M}} = 91.66$ kN. Throughout the report a ratio $V/V_{\mathrm{M}} = 0.0026$ is used for the simulations and the interaction diagram comparisons. For both the laboratory setups, the sample was prepared by mechanical vibration of the soil. This technique allowed to have dense or very dense samples. The relative density D_r, is calculated by interpreting small scale cone penetration test data with an empirical correlation. The average

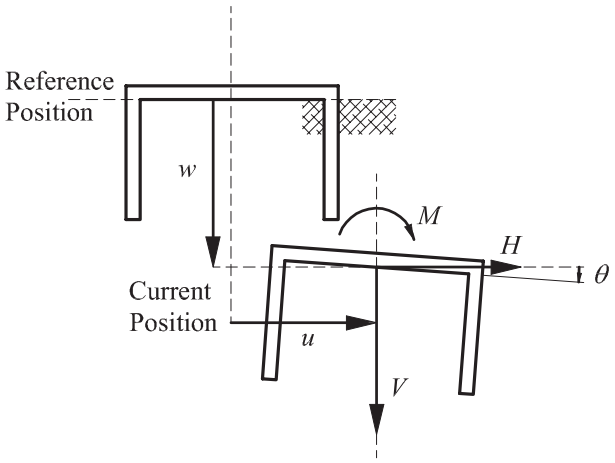

Figure 7: Sign conventions, after Butterfield et al. (1997)

D_r of the selected tests is 88.25%.

The sign convention for loads (V, H, M) and displacements (w, u, θ) is chosen according to the unified and consistent system proposed by Butterfield et al. (1997). Figure 7 depicts the sign conventions.

3 Analytical modelling

In this chapter the models used to interpret the experimental data are described. The calibration of some of the parameters is carried through on the base of the available experimental data. All assumptions and uncertainties are pointed out. Some points of discussion on the calibration of the parameters and on the model architecture are put forward.

3.1 Monotonic loading

3.1.1 Model architecture

The macro-element model of Nova and Montrasio (1991) is based on the classic framework of elasto-plasticity and was conceived to predict the mechanical response of a strip footing on a homogeneous soil layer under combined planar loading. The validity of the model was

then extended to different shallow foundations by Montrasio and Nova (1997), and to strip foundation under cyclic loading by di Prisco et al. (2003a). The model consists of five elements: elastic matrix, yielding surface, plastic potential, hardening law and flow rule. Following the rules of strain-hardening models the elements are combined to form the flexibility matrix $\boldsymbol{C}$, which relates the vector of normalised incremental displacements $d\boldsymbol{q}$, to the vector of normalised incremental forces $d\boldsymbol{Q}$:

$$d\boldsymbol{q} = \boldsymbol{C} d\boldsymbol{Q} \tag{1}$$

where $\boldsymbol{q}$ is the generalised vector of normalised displacements whereas $\boldsymbol{Q}$ is the generalised vector of normalised loads. $\boldsymbol{q}$ and $\boldsymbol{Q}$ are defined as:

$$\boldsymbol{q} = \begin{pmatrix} \eta \\ \varepsilon \\ \zeta \end{pmatrix} = V_{\mathrm{M}} \begin{pmatrix} w \\ \mu u \\ \psi D \theta \end{pmatrix} \tag{2}$$

$$\boldsymbol{Q} = \begin{pmatrix} \xi \\ h \\ m \end{pmatrix} = \frac{1}{V_{\mathrm{M}}} \begin{pmatrix} V \\ H/\mu \\ M/(\psi D) \end{pmatrix} \tag{3}$$

where μ and ψ are constitutive dimensionless parameters of the model.

Elasticity matrix The elasticity matrix, $\boldsymbol{K}_e$, is defined as:

$$\boldsymbol{K}_e = \mathrm{diag}(k_V, k_H, k_M) \tag{4}$$

Its elements are evaluated according to Doherty and Deeks (2003). To calculate the components of $\boldsymbol{K}_e$, an elastic modulus, $E = 25$ MPa, and a Poisson ratio, $\nu = 0.2$, are assumed.

Yielding surface The original yielding surface of the NMM is:

$$f = \left(\frac{H}{V_{\mathrm{M}}\mu}\right)^2 + \left(\frac{M}{D V_{\mathrm{M}} \psi}\right)^2 - \left(\frac{V}{V_{\mathrm{M}}}\right)^2 \left(1 - \frac{V}{V_{\mathrm{M}} \rho_c}\right)^{2\beta} \tag{5}$$

where ρ_c is the hardening parameter, V_{M} the bearing capacity of the foundation and β a constitutive parameter of the model. By substituting the load components according to eq. 3, eq. 5

becomes:

$$f = h^2 + m^2 - \xi^2 \left[1 - \left(\frac{\xi}{\rho_c}\right)\right]^{2\beta} \tag{6}$$

In the three-dimensional load space $(V - H - M/D)$ the yielding surface is an ellipsoid while in the three-dimensional normalised load space $(\xi - h - m)$ the yielding surface becomes a spheroid.

When using the strain-hardening plasticity frameworks it is typical to normalise the loads by V_0 which is the maximum vertical load ever applied to the foundation (Villalobos et al., 2009; Houlsby and Cassidy, 2002; Gottardi et al., 1999). This is apparently not the case in eq. 5. It should be clear though that $\rho_c = V_0/V_{\mathrm{M}}$ and, therefore, by simply substituting V_{M} with V_0/ρ_c, eq. 5 becomes normalised by V_0.

To include the contribution of the skirt to the resistance, eq. 5 is modified similarly to Villalobos et al. (2009):

$$f = \left(\frac{H}{V_{\mathrm{M}}\mu}\right)^2 + \left(\frac{M}{DV_{\mathrm{M}}\psi}\right)^2 - \left(\frac{V}{V_{\mathrm{M}}} + t_0\rho_c\right)^2 \left(1 - \frac{V}{V_{\mathrm{M}}\rho_c}\right)^{2\beta} \tag{7}$$

It is worth noting that by including t_0 in the formulation, the model has no longer a closed form solution.

Equation 7 differs from that of Villalobos et al. (2009) in three aspects. First, it is expressed by means of V_{M} and not V_0. Second, there is no term relative to the eccentricity of the surface in the $(H - M/D)$ load plane. The third and most substantial difference is that t_0 is not a function of V_0 and is defined as $V_{\mathrm{tM}}/V_{\mathrm{M}}$ where V_{tM} is the drained pull out resistance of the foundation.

V_{M} was found experimentally with test S64. To calculate V_{tM} a failure model in tension must be chosen. A pertinent failure model in tension is that in which the bucket foundation and the soil plug are involved in the pull out. As a result of that, the contributions of the pull out drained resistance are three: the buoyant weight of the foundation W'_{f}, the buoyant weight of the soil

plug W'_{p} and the tangential forces acting on the outer skirt. V_{tM} can then be expressed as follows:

$$V_{\mathrm{tM}} = 2\pi r_{\mathrm{o}} \int_0^d \tau_{\mathrm{o}} dx + W'_{\mathrm{f}} + W'_{\mathrm{p}} \tag{8}$$

where r_{o} is the outer radius of the foundation and τ_{o} is the shear stress along the wall. Obviously, V_{tM} (and thus t_0) is influenced by the choice of the soil-steel interface angle and the coefficient of lateral earth pressure. After scrupulous consideration and comparison with Villalobos (2006) a value of $t_0 = 0.007$ was taken. A more detailed discussion on t_0 is given in section 3.1.4.

The choice of using equation 7 is justified by the following observation. Standard dimensions of bucket foundations for real-scale OWTs are listed in Table 3 together with the load conditions suggested by Byrne (2013) and Lesny (2011). In Table 3, h is the load eccentricity, the subscripts "*w*" stands for waves and currents and the subscript "*wi*" stands for wind. To calculate the range of $M/(HD)$, the maximum M is divided by the minimum values of (HD) whereas the minimum M is divided by the maximum values of (HD). It should be mentioned though that most likely the real load paths will lie in the middle of the range and not in the region around the boundaries. In Figure 9 the loading path range for bucket foundations supporting OWTs is plotted together with the failure envelopes of Villalobos et al. (2009) and Nova and Montrasio (1991). To plot the envelope of Villalobos et al. (2009) the parameters of Ibsen et al. (2014), calibrated with small scale tests until failure, are adopted (except for t_0 which is set equal to 0.007). The parameters used to plot the envelope of the NMM are derived in section 3.1.2. In Figure 9 it is seen that in the sector of interest for OWTs the two envelopes give a fairly similar representation of the ultimate resistance. For the sake of completeness, it is worth to mention that the discrepancy between the two failure envelopes is exacerbated in the second quadrant. However, the load path is unlikely to lie on the second quadrant, unless V acts on the foundation with a large horizontal eccentricity.

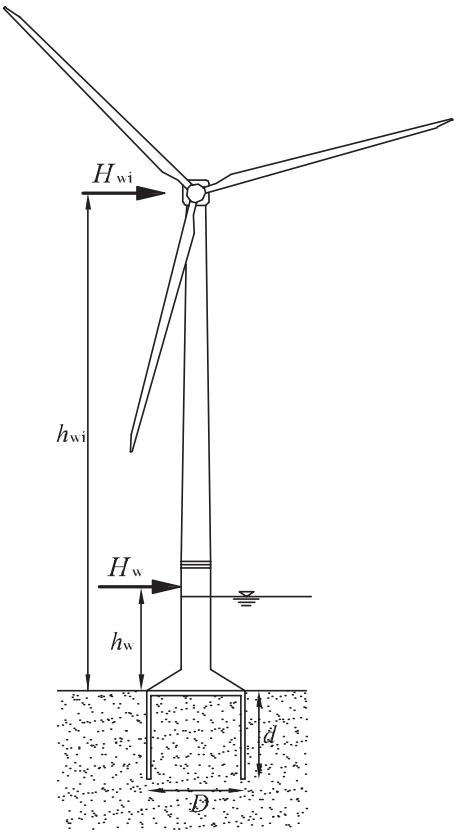

Figure 8: Sketch of an OWT

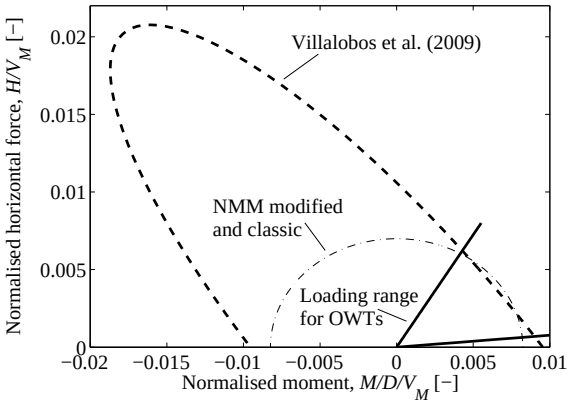

Figure 9: Benchmark of failure envelopes

Table 3: Range of features of a bucket foundation supporting a standard offshore wind turbine, (Byrne, 2011; Lesny, 2011)

Value	Unit	Maximum	Minimum
H_w	[MN]	10	3
H_{wi}	[MN]	2	1
h_w	[m]	40	20
h_{wi}	[m]	120	90
D	[m]	18	14
M	[MNm]	640	150
H	[MN]	12	4
V	[MN]	35	6
$M/(HD)$	[-]	11.43	0.69

Plastic potential In analogy with the yielding surface, the plastic potential differs from the original model only by the inclusion of the parameter t_0:

$$g = (\lambda h)^2 + (\chi m)^2 - (\xi + t_0\rho_g)^2 \left[1 - \left(\frac{\xi}{\rho_g}\right)\right]^{2\beta} \tag{9}$$

In eq. 9 ρ_g is a fictitious variable whereas λ and χ are constitutive dimensionless parameters.

Hardening law The hardening law is the rule by which the evolution of the hardening parameter, $d\rho_c$, is defined as a function of the increment of plastic displacements, $d\boldsymbol{q}_p$:

$$d\rho_c = (1-\rho_c)\frac{R_0}{V_{\mathrm{M}}}\left(d\eta + \frac{\alpha\,|d\varepsilon|}{\mu} + \frac{\gamma\,|d\zeta|}{\psi}\right) \tag{10}$$

In eq. 10, α and γ are constitutive dimensionless parameters while R_0 is the initial stiffness of the $V-w$ curve extrapolated in section 3.1.2. A discussion on the hardening law is proposed in section 3.1.5.

Flow rule The flow rule is consistent with the original model, and more generally, with the standard theory of plasticity. When the conditions $f=0$ and $df=0$ are fulfilled, the incremental plastic displacements $d\boldsymbol{q}_p$ can be expressed by:

$$d\boldsymbol{q}_p = \Lambda\frac{\partial g}{\partial \boldsymbol{Q}} \tag{11}$$

where Λ is the plastic multiplier.

3.1.2 Calibration of the modified NMM

Failure envelope (μ, ψ and β) The monotonic tests were run until failure of the geotechnical system. Thus, the yielding surface extrapolated is a failure surface ($\rho_c = 1$). Tests exploring the yielding surfaces were not possible with any of the experimental rig available. Hence, it is a fundamental assumption of the model that each and every yielding surface differs from the failure surface only in size, *i.e.* by the value of ρ_c. Moreover, to calibrate the failure envelope the variety of experiments was limited to only constant V tests with five different $M/(HD)$ ratios. This gives however sufficient information on the region of the load space ($V-H-M/D$) of interest for OWTs, *i.e.* V/V_{M} very close to the origin of the axes and loading paths with no change in V. The original (eqs. 5 and 6) and the modified (eq. 7) failure envelopes are calibrated with the same set of experimental data. Figure 10 shows two failure

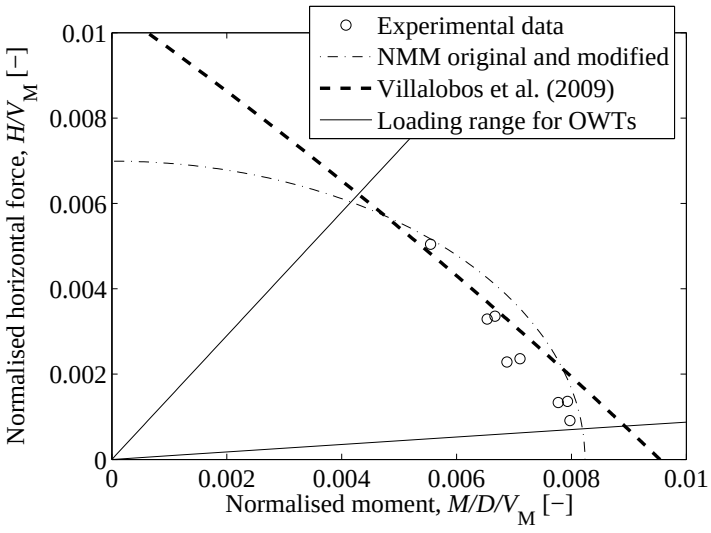

Figure 10: Calibration of the failure envelope of original and modified NMM on the base of experimental data

envelopes with the experimental points and the load range for OWTs in the normalised load plane ($H/V_{\mathrm{M}} - M/(DV_{\mathrm{M}})$) at $V/V_{\mathrm{M}} = 0.0026$. The two envelopes are that of Villalobos et al. (2009) with the parameters of Ibsen et al. (2014) and that of the modified NMM. The original NMM is calibrated in order to be equal to the modified NMM at $V/V_{\mathrm{M}} = 0.0026$. The purpose of that is to underline how essential the inclusion of t_0 is in the formulation of the model when trying to fit the experimental load-displacement curves with the two models, *cf.* section 3.1.3. Since the number of failure points is scarce, no best fit of the data is attempted. Rather, a conservative fit which encompasses all the experimental points is adopted. The parameter β is set equal to 0.95 as suggested in literature by Montrasio and Nova (1997). Appropriate values of μ and ψ for the modified yielding surface are 0.73 and 0.86 respectively.

$\mathbf{R_0}$ and $\mathbf{V_M}$ The bearing capacity of the foundation, V_{M}, and the initial vertical stiffness, R_0, can be extrapolated from the $V - w$ curve of test S64. Such curve is shown in Figure 11. The value of V at the end of the skirt penetration (point A in Figure 11) is the result of the

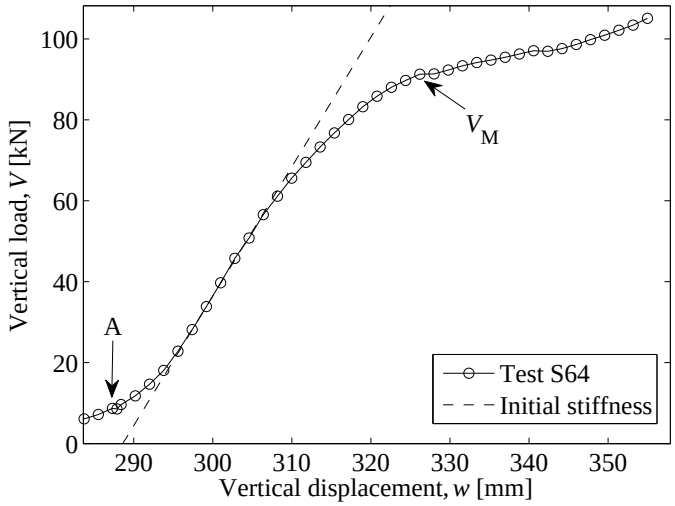

Figure 11: Experimental $V - w$ curve, and fit of the initial stiffness

reaction vertical forces due to tip end bearing and wall friction. By fitting with a straight line the initial points of the curve, R_0 is evaluated as 3202 kN/m. Strictly speaking, this value of R_0 is not accurate. To gain the exact value of R_0 the foundation should be unloaded as soon as full penetration is achieved and then re-loaded. During test S64 no unloading phase was performed after full penetration of the foundation. Nevertheless, the precision of R_0 is considered sufficient for the scope of the paper.

In Figure 11 a local shear failure of the soil can be observed in correspondence to an abrupt change in stiffness ($w = 326.2$ mm). V_{M} is taken equal to 91.66 kN.

α, γ, λ and χ As elucidated in Nova and Montrasio (1991), to calibrate the parameters of the potential and of the hardening rule, pure H and pure M tests are necessary. Although, when the load eccentricity ratio $M/(HD)$ exceeds a certain value, the behaviour of the foundation is no longer significantly affected by the increase of vertical eccentricity (see test S27 and S28 in Figure 4). This applies to both load-displacement curves and displacement trajectory curves. Evidence of such response is given in Figure 12, where the standard NMM with standard

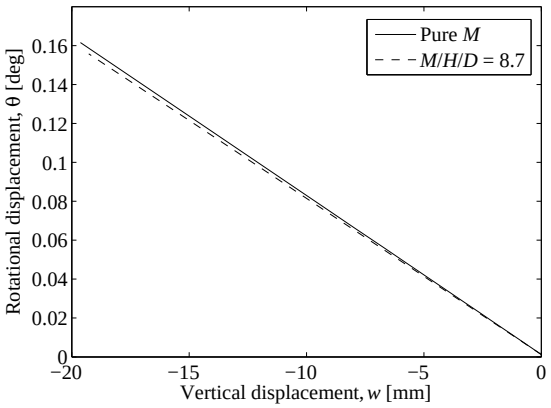

Figure 12: Displacement trajectory of a pure *M* test and a $M/(HD) = 8.7$ test simulated with the original NMM

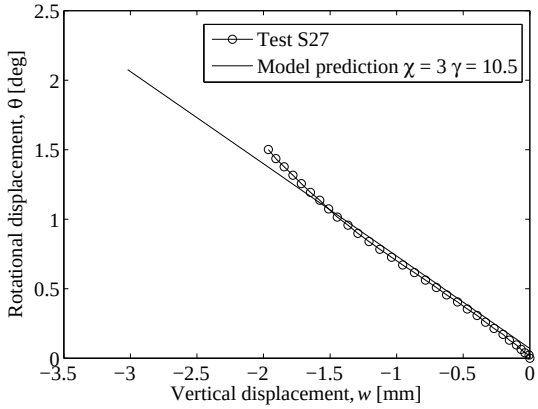

Figure 13: Displacement trajectory of test S27 against model prediction to extrapolate χ and γ

parameters is used to predict a pure M ($M/(HD) = \infty$) test and a test with $M/(HD)$ = 8.7. The two trajectories match very well, meaning that the test with $M/(HD)$ = 8.7 (test S27), can be used instead of a pure M test to calibrate χ and γ. Two parameters that give a reasonable fit of the $\theta - w$ trajectory are χ = 10.5 and γ = 3 (*cf.* Figure 13).

The other two parameters, namely α and λ, are evaluated by conducting a parametric study trying to match the load-displacement curves and the displacement trajectories of the available tests. Appropriate values for α and λ are 11 and 10.5 respectively.

3.1.3 Model validation

The parameters of the original NMM are evaluated with the same procedure explained in section 3.1.2 for the modified NMM. As shown in Figure 14, by using the original NMM, the load-displacement curves achieved cannot simulate the experimental data. By adopting the modified version of the NMM, both load-displacement curves and displacement trajectories curves are reasonably well predicted (*cf.* Figure 15 - Figure 30). As expected, not all tests are equally well represented by the model. Nonetheless, it is partly reassuring to note that the largest deviation

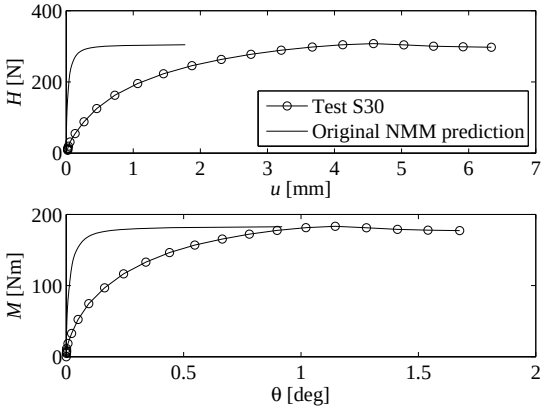

Figure 14: Original NMM prediction of test S30

between analytical and experimental results is found in those curves which are most affected by the parameters gained by trial and error procedure (u-w trajectories of Figure 24 and Figure 26). Also the M-θ curves of the same tests (Figure 23 and Figure 25) are overpredicted by the model. The displacement trajectory θ-w, which was more rationally calibrated, appears to be consistent throughout the entire tests series. This observation however, does not exclude a possible weak point of the model when dealing with the prediction of the u-w trajectories.

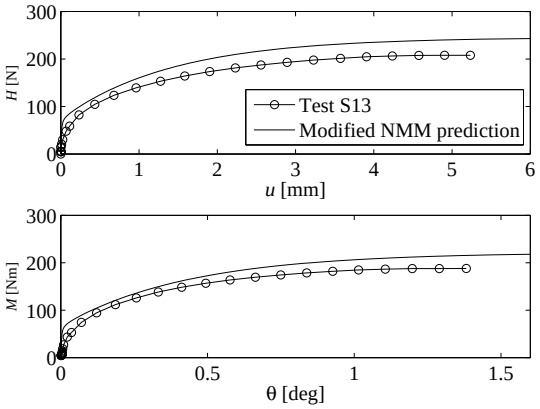

Figure 15: Modified NMM prediction of test S13, load-displacement curves

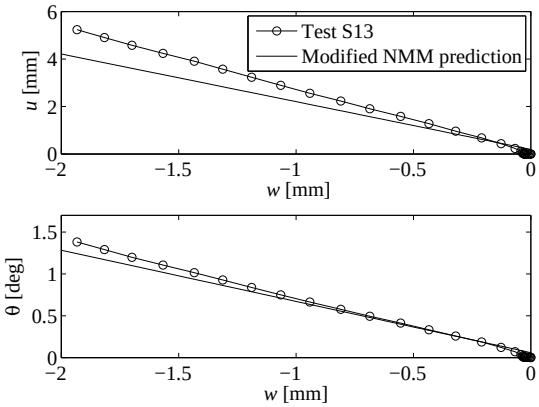

Figure 16: Modified NMM prediction of test S13, displacement trajectories

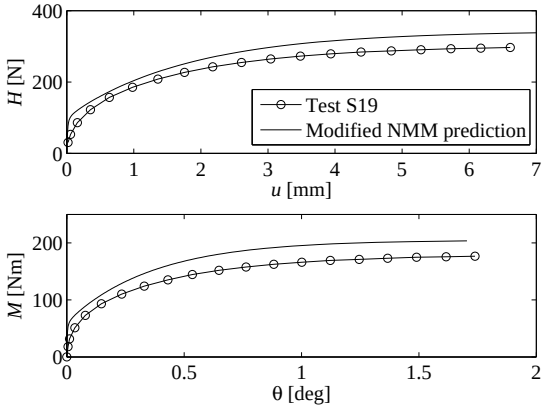

Figure 17: Modified NMM prediction of test S19, load-displacement curves

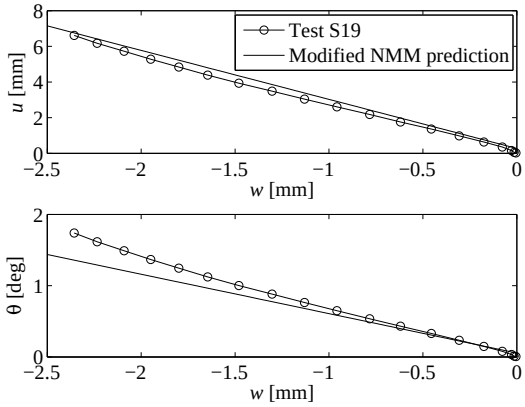

Figure 18: Modified NMM prediction of test S19, displacement trajectories

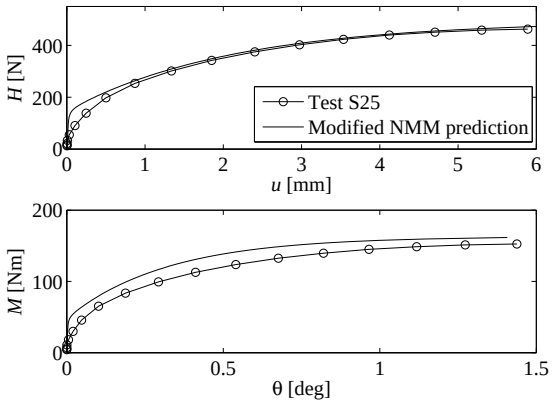

Figure 19: Modified NMM prediction of test S25, load-displacement curves

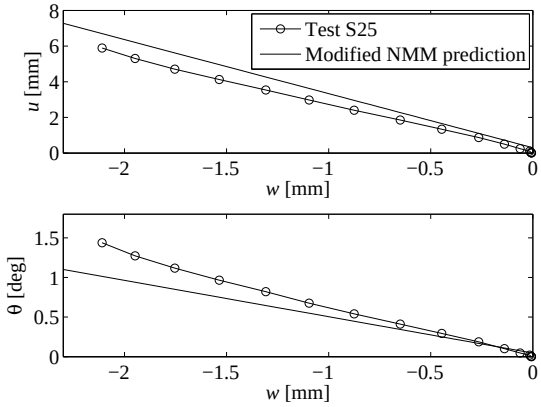

Figure 20: Modified NMM prediction of test S25, displacement trajectories

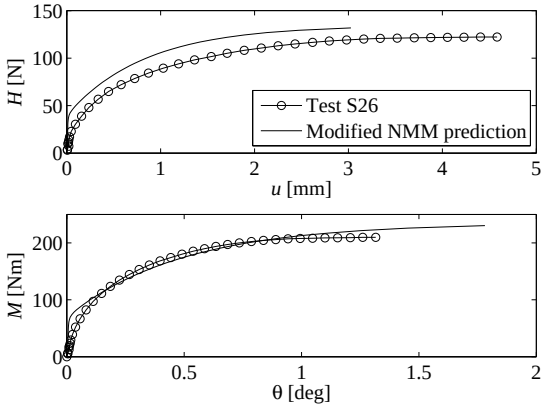

Figure 21: Modified NMM prediction of test S26, load-displacement curves

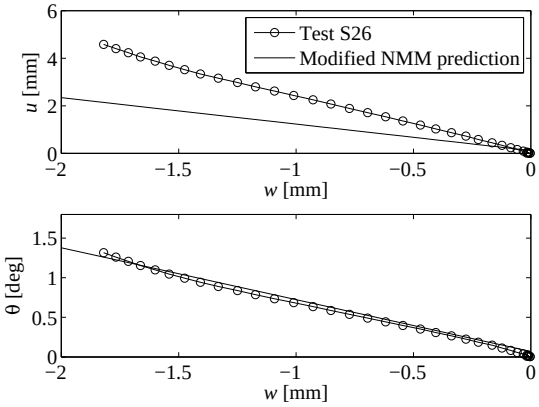

Figure 22: Modified NMM prediction of test S26, displacement trajectories

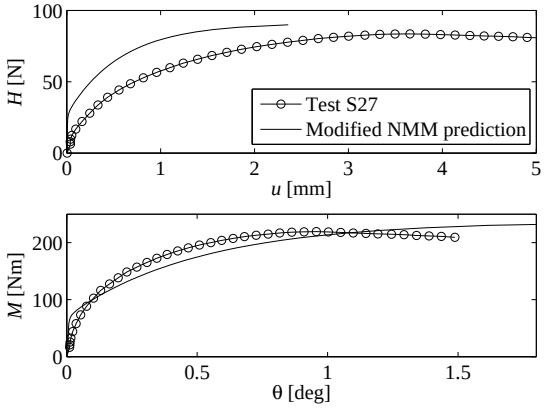

Figure 23: Modified NMM prediction of test S27, load-displacement curves

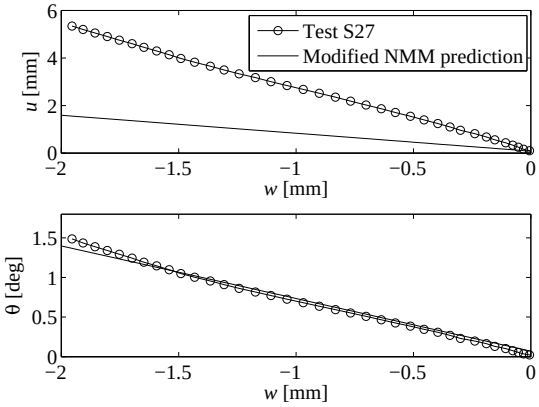

Figure 24: Modified NMM prediction of test S27, displacement trajectories

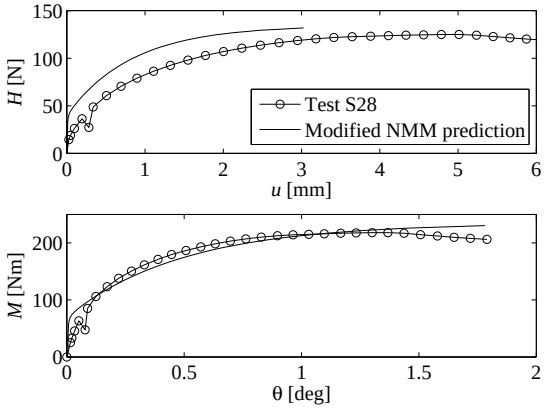

Figure 25: Modified NMM prediction of test S28, load-displacement curves

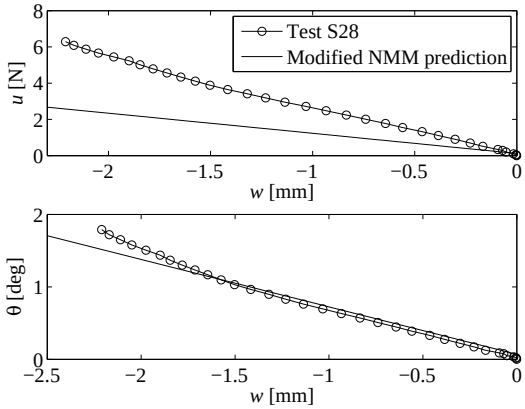

Figure 26: Modified NMM prediction of test S28, displacement trajectories

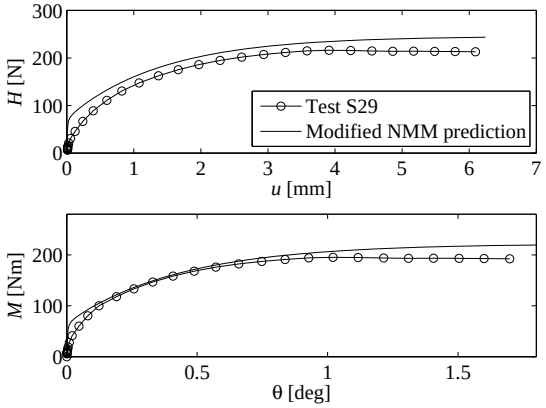

Figure 27: Modified NMM prediction of test S29, load-displacement curves

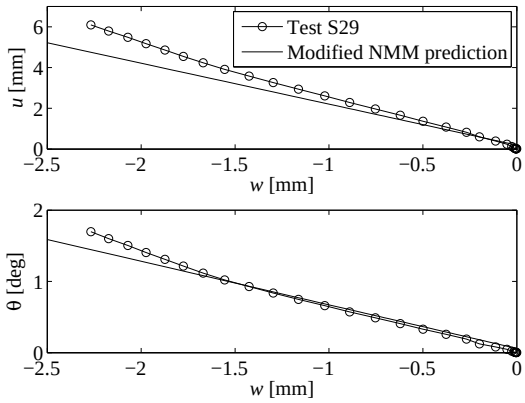

Figure 28: Modified NMM prediction of test S29, displacement trajectories

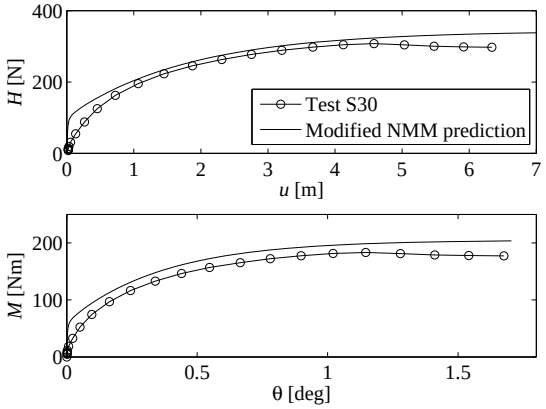

Figure 29: Modified NMM prediction of test S30, load-displacement curves

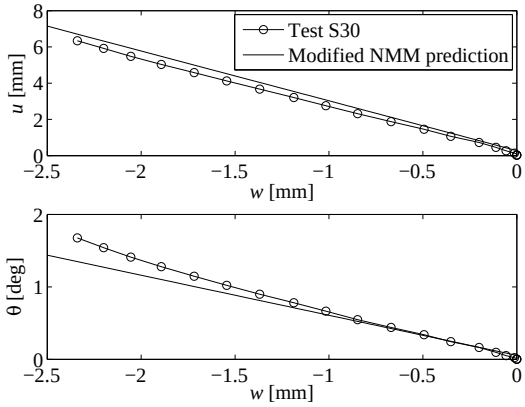

Figure 30: Modified NMM prediction of test S30, displacement trajectories

The incapability of the original NMM to reproduce the experimental results is attributed to the radically different way in which the yielding surface expands in the two models during monotonic loading. As shown in Figure 31, when using the original NMM, there is no gradual transition from one yielding surface to the other. All the yielding surfaces tend to collapse onto one envelope. When including t_0 in the model formulation (see Figure 32), the path towards failure shows a much more gradual evolution of the yielding surface than the original NMM. This observation is true when $V/V_{\mathrm{M}} \approx 0$. In case $V/V_{\mathrm{M}} > 0$, for example for oil and gas platforms, the effect of t_0 would be negligible and the original NMM could perhaps be able to predict the response.

The parameters of the modified NMM used to match the experimental curves are summarised in Table 4.

3.1.4 Discussion on t_0

The tension parameter, t_0, was introduced for the first time by Villalobos (2006) as a function of V_0 ($t_0 = V_{\mathrm{tM}}/V_0$). t_0 was essential to his study to define a yielding surface capable to describe loads in tension. This surface was then employed in a hyperplastic macro-model by Nguyen-

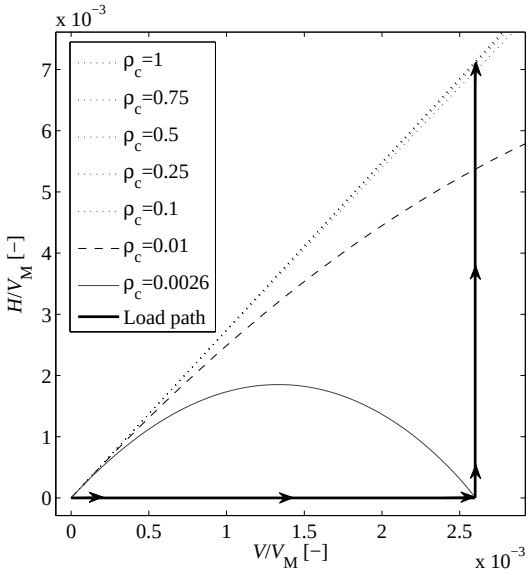

Figure 31: Yielding surface evolution for the original NMM

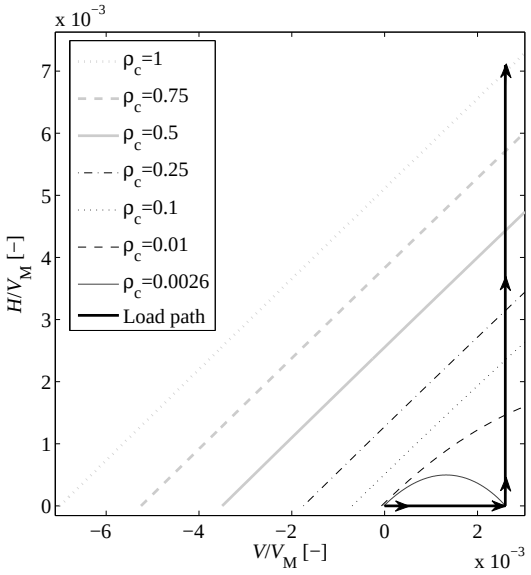

Figure 32: Yielding surface evolution for the modified NMM

Table 4: Parameters of the modified NMM

μ [-]	ψ [-]	β [-]	α [-]	γ [-]	χ [-]	λ [-]	t_0 [-]	V_{M} [kN]	R_0 [kN/m]
0.73	0.86	0.95	11	10.5	3	3.5	0.007	91.66	3202

.

Sy (2006). To not overcomplicate the model Nguyen-Sy (2006) set t_0 constant. In the model presented here, t_0 is also kept constant but is calculated with the ultimate bearing capacity V_{M} instead of V_0. As a result, the value of t_0 evaluated in this work is one order of magnitude smaller than that of Villalobos (2006) and Nguyen-Sy (2006). Letting t_0 vary according to the development of the yielding has not been attempted here but would perhaps be of interest.

3.1.5 Discussion on the hardening law

All the tests carried out at such a small value of V/V_{M} showed uplift ($w < 0$) instead of settlement ($w > 0$). It should be clarified that this kind of behaviour cannot be an artefact of the experimental rig since the same finding is reported in Villalobos et al. (2009). The theory

behind the macro-element approach defines each yielding surface as uniquely associated with a value of the hardening parameter. This is properly elucidated, and put into concrete, in Gottardi et al. (1999) who plotted back-calculated $V - w_{\mathrm{p}}$ curves from radial displacement and constant V tests against the hardening law (where w_{p} is the irreversible vertical displacement). Obviously, the same procedure would not be possible here since the hardening law involves all three components of the plastic displacement. A hardening law merely based on a compressive $V-w$ curve would be not theoretically compatible with loading paths close to the axes origin as there, for bucket foundations, uplift instead of settlement occurs. In the opinion of the authors this aspects should be further investigated.

3.2 Cyclic loading

In this section a simplified version of the boundary surface model developed by di Prisco et al. (2003a) is presented (see also di Prisco et al., 2003b; di Prisco et al., 2006; Buscarnera et al., 2010). Originally, the model in question was designed to simulate the response of shallow foundations subjected to a planar earthquake excitation. The version of the model presented here is conceived to reproduce the behaviour of foundations under sinusoidal M and H with constant V. As a result of that, the model is simplified and some of its elements are neglected. The constitutive parameters are estimated by trial and error against the experimental results.

3.2.1 Model architecture

Let us assume that a point of the load space Q (ξ_{Q}, h_{Q}, m_{Q}) represents the current load state. Boundary surface models define the amount of cyclic displacement for each load step as a function of the distance between Q and an image point, I (ξ_{I}, h_{I}, m_{I}), that lies on a defined boundary surface (see Figure 33). In the model presented here, the boundary surface coincides with the yielding surface while the image point is identified with an appropriate mapping rule

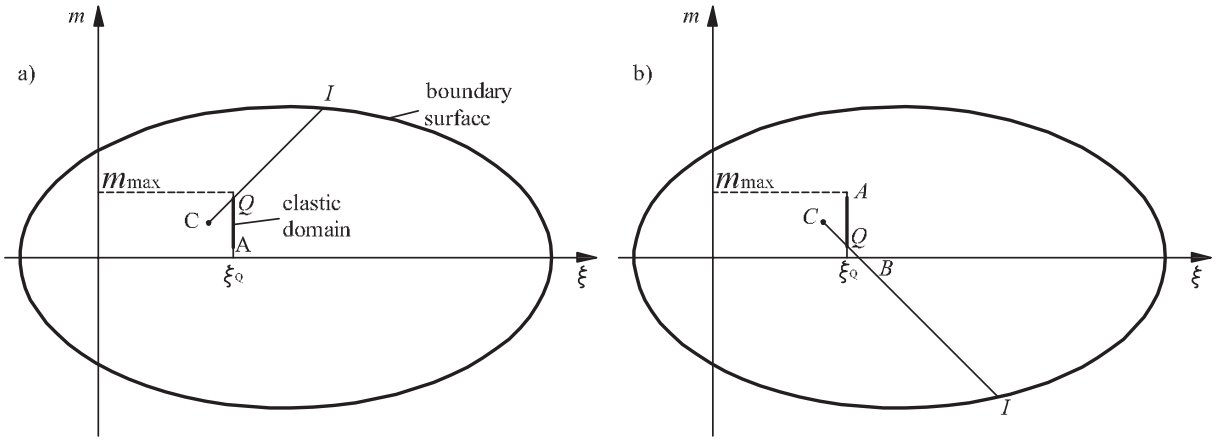

Figure 33: Sketch of the mapping rule for the definition of δ, a) $dm > 0$, $m_{\mathrm{I}} > 0$ and $m_{\mathrm{Q}} > 0$; b) $dm < 0$, $m_{\mathrm{I}} < 0$ and $m_{\mathrm{Q}} > 0$. Elastic domain and boundary surface in bold solid line

explained in the following. The model is integrated into the NMM framework by means of the matrix $\mathbf{\Phi}$ which is incorporated into the flow rule as follows:

$$d\boldsymbol{q}_p = \Lambda \mathbf{\Phi} \frac{\partial g}{\partial \boldsymbol{Q}} \tag{12}$$

The matrix $\mathbf{\Phi}$ is diagonal and its elements are defined as:

$$\Phi_{ii} = exp\left(-\alpha_i \sqrt{\frac{\delta \rho_c}{\xi}}\right) exp\left(-\beta_i \rho_k\right) \tag{13}$$

where α_i and β_i are constitutive parameters, ρ_k is a variable updated as ρ_c (eq. 10) and δ is a function of the distance between the current load state Q and the image point on the boundary surface, I. To describe how the mapping rule works, a sketch of the normalised load plane ($m - \xi$) is illustrated in Figure 33. For simplicity, a two dimensional load path with $0 < m_{\mathrm{Q}} < m_{\mathrm{max}}$ is chosen. An elastic domain in which no irreversible displacements can occur, is defined by means of the segment AQ which is a portion of the total load path. In this study it was deliberately chosen to set the elastic domain equal to the 75% of the total load path. According to the sign of dm, the point C (ξ_{C}, h_{C}, m_{C}), which is necessary to discover the position of I, has coordinates:

$$\xi_{\mathrm{C}} = \xi_{\mathrm{Q}} - QA/2 \tag{14}$$

$$m_{\mathrm{C}} = \begin{cases} m_{\mathrm{Q}} - QA/2 & \text{for } dm > 0 \\ m_{\mathrm{Q}} + QA/2 & \text{for } dm < 0 \end{cases} \tag{15}$$

The straight line connecting C to Q identifies the image point I on the boundary surface. The point of intersection between the line CI and the ξ axis is named B. The variable δ is defined as follows:

$$\delta = \begin{cases} CB + \phi BI & \text{for } m_{\mathrm{I}} < 0 \text{ and } m_{\mathrm{Q}} > 0 \\ CB + \phi BI & \text{for } m_{\mathrm{I}} > 0 \text{ and } m_{\mathrm{Q}} < 0 \\ CI & \text{for } m_{\mathrm{I}} < 0 \text{ and } m_{\mathrm{Q}} < 0 \\ CI & \text{for } m_{\mathrm{I}} > 0 \text{ and } m_{\mathrm{Q}} > 0 \end{cases} \tag{16}$$

where ϕ is a constitutive dimensionless parameter of the model. The second condition of equation 16 never occurs within the loading paths modelled in this study. Nevertheless, it is included for the sake of completeness.

The original boundary surface model of di Prisco et al. (2003a) includes a further element, namely the memory surface. Since the loading conditions are such that M and H are periodic with constant amplitude, the memory surface is not necessary to the model definition.

The boundary surface model presented introduces 7 new non-dimensional parameters. As yet, it is unclear how to calibrate these parameters in a systematic way. However, in the following section, the results of a parametric study aimed at fitting the experimental long-term rotation and horizontal displacement of the foundation is shown.

3.2.2 Model validation

In Figures 34 and 35 the load-displacement curves of test C16 evaluated with the model are shown. By comparison with Figures 5 and 6, it can be observed that some features of the cyclic behaviour are properly simulated by the model: after each load cycle, the displacement components accumulate, the accumulation rate decreases and the area of the hysteresis loops becomes smaller. On the other hand, the model is unable to reproduce the increase in tangent stiffness as a function of *N* and the overlapping of hysteretic loops. The change in stiffness can be incorpo-

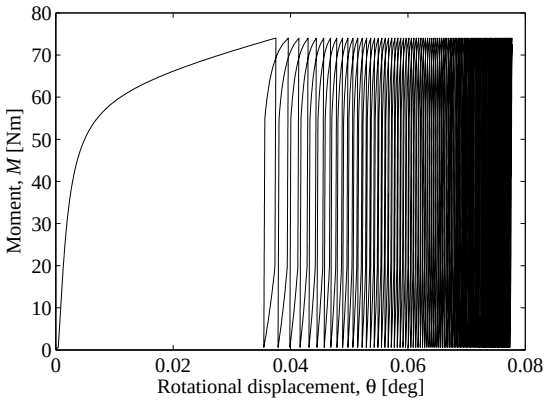

Figure 34: $M - \theta$ curve of the model simulating test C16, first 100 cycles

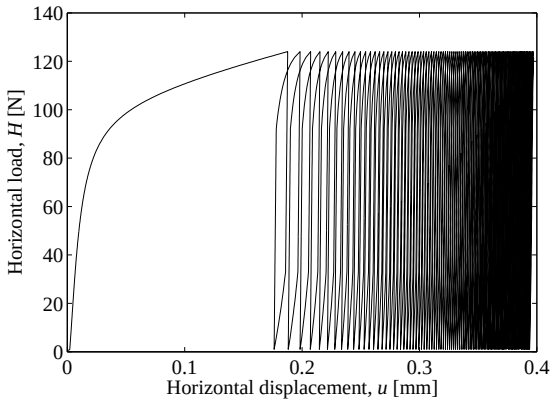

Figure 35: $H - u$ curve of the model simulating test C16, first 100 cycles

rated into the model by deriving an experimentally based updating rule for $\boldsymbol{K}_e$. However, this was not attempted in the present study as the long-term accumulated displacements, rather than the change in unloading-reloading stiffness, was the main aim of the modelling. Figures 36-45 compare the experimental results with the model simulations. In order to neutralise the inaccuracy of the monotonic response and thereby analyse the cyclic modelling independently of the monotonic behaviour, the long-term accumulated displacements of experimental and analytical results are compared in terms of normalised displacements. The normalised rotation is defined as $(\theta_{\mathrm{N}} - \theta_0)/\theta_0$, where θ_{N} is the rotational displacement at cycle N and θ_0 is the rotational displacement at the first load cycle. The same definition applies to the normalised horizontal displacement, but with u instead of θ. Note that for the analytical model, $\theta_0 = \theta_s$ and $u_0 = u_s$, where the subscript "s"indicates the displacements on the monotonic curve corresponding to M_{max}. The experimental tests, even though were performed in substantially drained condition, do not strictly satisfy this condition.

The parameters governing the cyclic behaviour are determined by trial and error from the four experimental cyclic tests. The macro-model appears to have good prediction abilities of the normalised accumulated displacements u and θ.

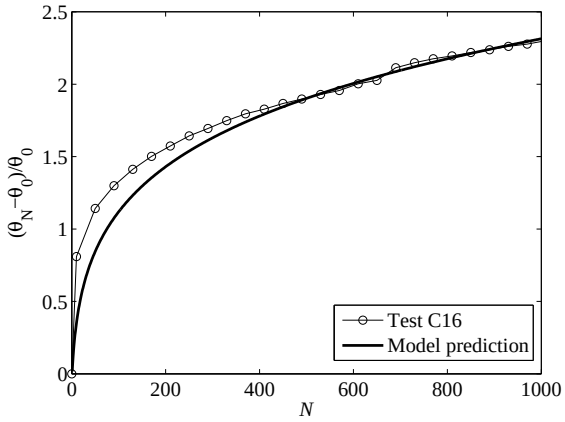

Figure 36: Accumulated rotational displacement of the first 1000 cycles, experimental and analytical results for test C16

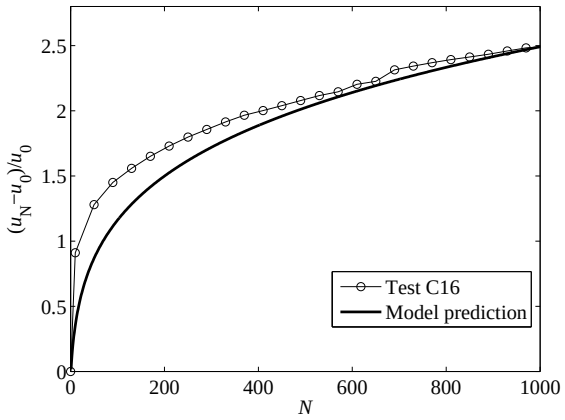

Figure 37: Accumulated horizontal displacement of the first 1000 cycles, experimental and analytical results for test C16

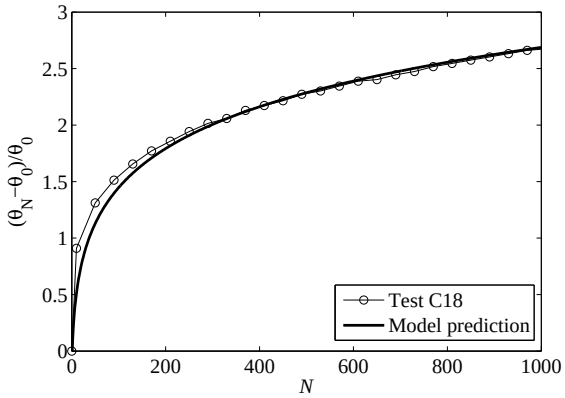

Figure 38: Accumulated rotational displacement of the first 1000 cycles, experimental and analytical results for test C18

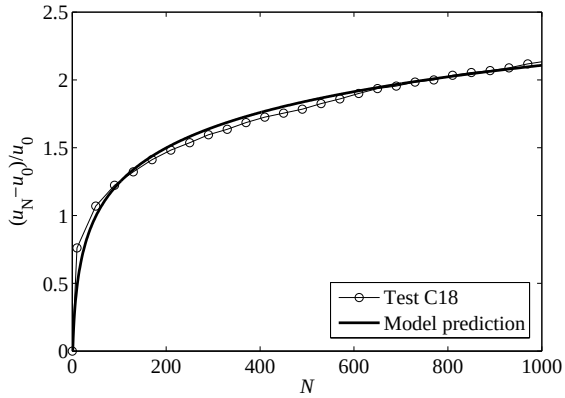

Figure 39: Accumulated horizontal displacement of the first 1000 cycles, experimental and analytical results for test C18

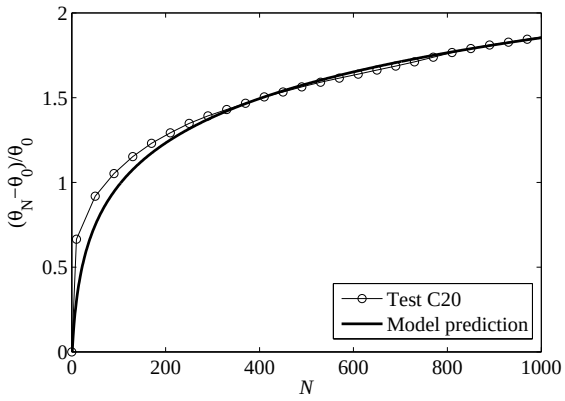

Figure 40: Accumulated rotational displacement of the first 1000 cycles, experimental and analytical results for test C20

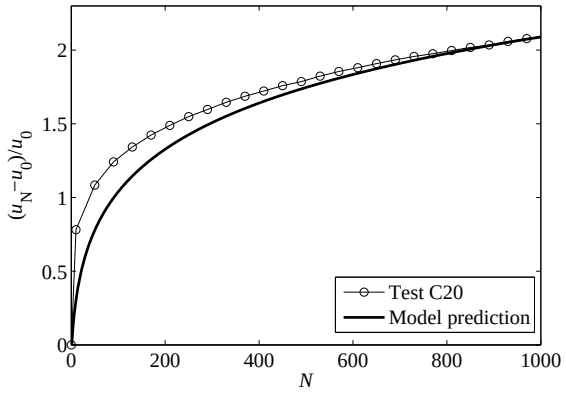

Figure 41: Accumulated horizontal displacement of the first 1000 cycles, experimental and analytical results for test C20

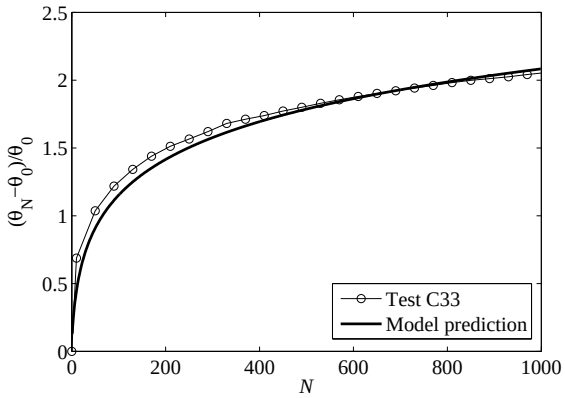

Figure 42: Accumulated rotational displacement of the first 1000 cycles, experimental and analytical results for test C33

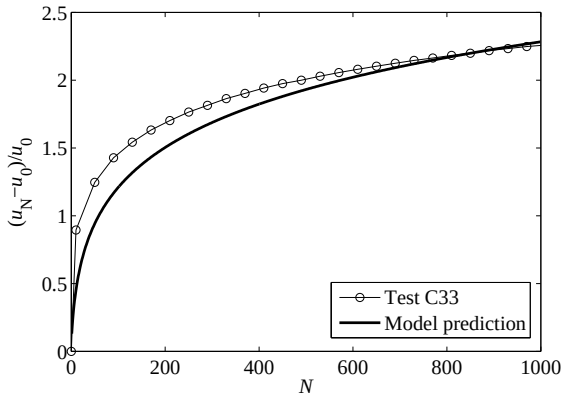

Figure 43: Accumulated horizontal displacement of the first 1000 cycles, experimental and analytical results for test C33

To achieve a proper quantitative match of the experimental results, the cyclic parameters related to u and θ have necessarily to be changed for each simulation. The parameters used in the simulations are listed in Table 5. Figure 44 shows how the parameters vary as a function of the cyclic loading magnitude ratio, $M_{\text{max}}/M_{\text{R}}$. A clear decreasing trend of the parameters for increasing $M_{\text{max}}/M_{\text{R}}$ can be observed. By including more tests in the analysis, also the dependency of the parameters on the cyclic loading ratio, $M_{\text{min}}/M_{\text{max}}$, might be obtained. By slightly adjusting the

parameters, the displacements at number of cycles larger than 1000 can also be predicted (*cf.* Figures 45 and 46).

The reason of the variability of the parameters of the boundary surface model is to be found in how the mapping rule is defined. It is likely that a more sophisticated mapping rule would be able to capture the normalised displacements avoiding the dependency of the parameters on the loading path.

Table 5: Parameters of the boundary surface model

Test	α_V	α_H	α_M	β_V	β_H	β_M	ϕ
C16	350	5	5	70	6	6	0.01
C18	350	14	14	70	43	39	0.01
C20	350	13	13	70	27	29	0.01
C33	350	7	7	70	16	17	0.01

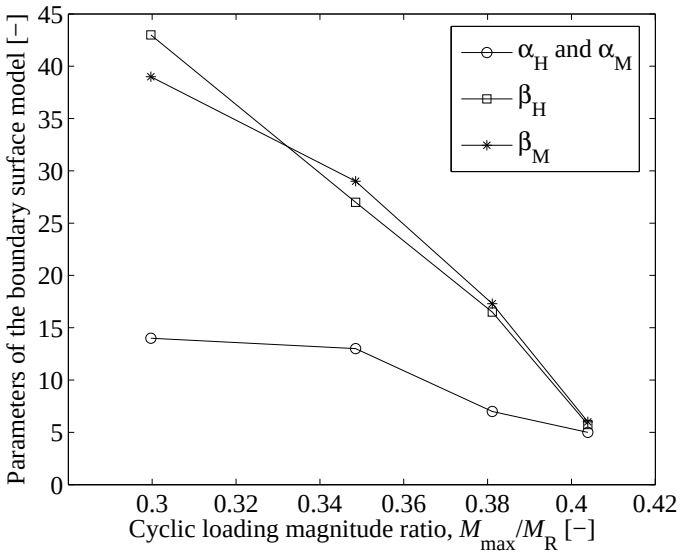

Figure 44: Parameters of the boundary surface model as a function of the cyclic loading magnitude ratio

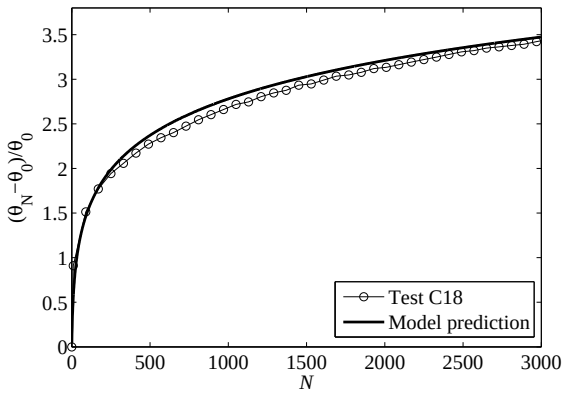

Figure 45: Rotational accumulated displacement of the first 3000 cycles, experimental and analytical results for test C18

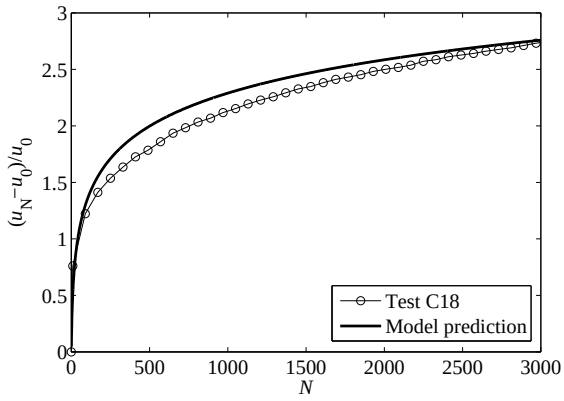

Figure 46: Horizontal accumulated displacement of the first 3000 cycles, experimental and analytical results for test C18

4 Conclusions and future work

In this work the possibility of interpreting experimental tests of bucket foundations under monotonic and cyclic loading with a macro-element model is explored. The problem investigated concerns monopod bucket foundations supporting offshore wind turbines. The well-known model of Nova and Montrasio (1991) is slightly modified and used to interpret a series of monotonic experimental tests. To account for cyclic loading, the model is integrated with a simplified version of the boundary surface model of di Prisco et al. (2003a). Both monotonic and cyclic experimental data are fairly well predicted by the analytical simulations.

Some aspects of the modelling should be further investigated. As emphasised in one of the put forward discussions, the expression of an appropriate hardening law is not an easy task due to the uplift event occurring under general loading at $V/V_{\mathrm{M}} \approx 0$. This issue should be properly addressed. Furthermore, as pointed out in Byrne (2000) and Larsen (2008), close to the origin of the load space the failure locus can be approximated as linear. This could probably be included in the model and reduce the complexity of the approach. Regarding the cyclic

loading modelling, the parameters of the boundary surface model were found to be affected by the loading path. As a result of that, the analysis of additional cyclic loading tests would be necessary to provide the functions related to the parameters. Another way to generalise the model would be to attempt a modification of the mapping rule. Furthermore, the combination of different load packages would be a crucial feature to be included in the model to obtain more realistic responses. Finally, since the model is validated against small-scale experiments, its applicability to real design situations is to be excluded until centrifuge tests or large-scale tests will corroborate the findings of this study.

Abbreviations

OWTs	offshore wind turbines
NMM	Nova and Montrasio (1991) model

Nomenclature

d	length of the skirt
f	yielding function
g	plastic potential
f_l	loading frequency
h	load eccentricity
k_V,k_H,k_M	components of $\boldsymbol{K}_e$
$\boldsymbol{q}$	vector of normalised displacements
r_o	outer radius of the foundation
t	wall thickness
t_l	lid thickness
u	horizontal displacement
u_0	horizontal displacement of the first cycle
u_s	horizontal displacement on the monotonic curve corresponding to M_{max}
w	vertical displacement
w_p	plastic vertical displacement
A,Q,I,C,B	points of the normalised load space used for the mapping rule description
$\boldsymbol{C}$	flexibility matrix

D	foundation diameter
D_{r}	relative density
E	elastic modulus
H	horizontal load
$\boldsymbol{K}_e$	elasticity matrix
$\boldsymbol{Q}$	vector of normalised loads
V	vertical load
V_{M}	bearing capacity of the foundation
V_{tM}	tensile capacity
V_0	preconsolidation vertical load
M_{R}	monotonic moment capacity
M_{max}, M_{min}	maximum and minimum cyclic moment
N	number of cycles
W	self-weight of the foundation
W'_{f}	buoyant weight of the foundation
W'_{p}	buoyant weight of the soil
α_V,α_H,α_M,β_V,β_H,β_M,ϕ	parameters of the boundary surface model
μ,ψ,β,λ,χ,α,γ,R_0,t_0	parameters of the modified NMM
ε	normalised horizontal displacement
ζ	normalised rotational displacement
η	normalised vertical displacement
θ	rotational displacement
θ_0	rotational displacement of the first cycle
θ_s	rotational displacement on the monotonic curve corresponding to M_{max}
ξ	normalised vertical load
δ	variable governing the mapping rule
ν	poisson ratio
ρ_c	hardening parameter
ρ_g	fictitious variable of the plastic potential
ρ_k	updating variable of the boundary surface model
τ_o	shear stresses acting over the skirt
Λ	plastic multiplier
$\boldsymbol{\Phi}$	matrix governing the cyclic displacements accumulation
Φ_{ii}	components of $\boldsymbol{\Phi}$

References

Bienen, B., Byrne, B. W., Houlsby, G. T. and Cassidy, M. J. (2006). Investigating six-degree-of-freedom loading of shallow foundations on sand. *Géotechnique* 56, No. 6, 367-379

Buscarnera, G., Nova, R., Vecchiotti, M., Tamagnini, C. and Salciarini, D. (2010). Settlement analysis of wind turbines. In *Soil-Foundation-Structure Interaction*, Orense et al. (Eds). CRC Press

Butterfield, R. and Ticof, J. (1979). The use of physical models in design. In *Proceedings of the 7th European Conference on Soil Mechanics*, Brighton, 259-261

Butterfield, R., Houlsby, G. T. and Gottardi, G. (1997). Standardized sign conventions and notation for generally loaded foundations. *Géotechnique* 47, No. 5, 1051-1054

Byrne, B. W. (2000). *Investigations of suction caissons in dense sand*. Ph.D. thesis, Oxford University

Byrne, B. W. and Houlsby, G. T. (2001). Observation of footing behaviour on loose carbonate sand. *Géotechnique* 51, No. 5, 463-466

Byrne, B. W. (2011). *Foundation Design for Offshore Wind Turbines*. Géotechnique lecture

Chatzigogos, C. T., Figini, R., Pecker, A. and Salençon, J. (2011). A macroelement formulation for shallow foundations on cohesive and frictional soils. *International Journal for Numerical and Analytical Methods in Geomechanics* 35, No. 8, 902-931

Cremer, C., Pecker, A. and Davenne, L. (2001). Cyclic macro-element for soil-structure interaction: material and geometrical non-linearities. *International Journal for Numerical and Analytical Methods in Geomechanics* 25, No. 13, 1257-1284

di Prisco, C., Nova ,R. and Sibilia, A. (2003a). Shallow footing under cyclic loading: experimental behaviour and constitutive modeling. In *Geotechnical analysis of seismic vulnerability of historical monuments*, Maugeri M. and Nova R. (Eds). Patron, Bologna

di Prisco, C., Nova, R., Perotti, F. and Sibilia, A. (2003b). Analysis of soil-foundation interaction of tower structures under cyclic loading. In *Geotechnical analysis of seismic vulnerability of historical monuments*, Maugeri M. and Nova R. (Eds). Patron, Bologna

di Prisco, C., Massimino, M. R., Maugeri, M., Nicolosi, M. and Nova, R. (2006). Cyclic numerical analyses of Noto Cathedral: soil-structure interaction modelling. *Rivista Italiana di Geotecnica* 2, 49-63

di Prisco, C. (2012). Cyclic mechanical response of rigid bodies interacting with sand strata. In *Mechanical Behaviour of Soils under Environmentally Induced Cyclic Loads*, di Prisco C. and Wood D. M. (Eds). CISM, Udine

Doherty, J. P. and Deeks, A. J. (2001). Elastic response of circular footings embedded in a non-homogeneous half-space. *Géotechnique* 53, No. 8, 703-714

Foglia, A., Ibsen, L. B., Nicolai, G., and Andersen, L. V. (2014). Observations on bucket foundations under cyclic loading in dense saturated sand. In *Proceedings of the 8th international conference of physical modelling in geotechnics (ICPMG), Perth*, Gaudin C. and White D. (Eds.). CRC Press

Gottardi, G. and Butterfield, R. (1993). On the bearing capacity of surface footings on sand under general planar loads. *Soils and Foundations* 33, No. 3, 68-79

Gottardi, G. and Butterfield, R. (1995). The displacement of a model rigid surface footing on dense sand under general planar loading. *Soils and Foundations* 35, No. 3, 71-82

Gottardi, G., Houlsby, G. T. and Butterfield, R. (1999). Plastic response of circular footings on sand under general planar loading. *Géotechnique* 49, No. 4, 453-469

Govoni, L., Gourvenec, S, and Gottardi, G. (2011). A centrifuge study on the effect of embedment on the drained response of shallow foundations under combined loading. *Géotechnique* 61, No. 12, 1055-1068

Haigh, S. K. (2014). Foundations for offshore wind turbines. In *Proceedings of the 8th Inter-*

national Conference of Physical Modelling in Geotechnics (ICPMG), Perth, Gaudin C. and White D. J. (Eds). CRC Press

Houlsby, G. T. and Cassidy, M. J. (2002). A plasticity model for the behaviour of footings on sand under combined loading. *Géotechnique* 52, No. 2, 117-129

Houlsby, G. T. and Puzrin, A. M. (2007). *Principles of Hyperplasticity*. Springer

Ibsen, L. B., Larsen, K. A. and Barari, A. (2014). Calibration of Failure Criteria for Bucket Foundations on Drained Sand under General Loading. *Journal of Geotechnical and Geoenvironmental Engineering* 140, No. 7

Larsen, K. A. (2008). *Static behaviour of bucket foundations*. Ph.D. thesis, Aalborg University

LeBlanc, C., Byrne, B. W. and Houlsby, G. T. (2010). Response of stiff piles in sand to long-term cyclic lateral loading. *Géotechnique* 60, No. 2, 79-90

Lesny, K. (2011). *Foundations for Offshore Wind Turbines - Tools for Planning and Design*. VGE Verlag GmbH

Kafle, B. and Wuttke, F. (2013). Cyclic macroelement for shallow footing over unsaturated soil. In *Advances in Unsaturated Soils*, Caicedo et al. (Eds). CRC Press

Martin, C. M. (1994). *Physical and numerical modelling of offshore foundations under combined loads*. Ph.D. thesis, Oxford University

Montrasio, L. and Nova, R. (1997). Settlement of shallow foundations on sand: geometrical effects. *Géotechnique* 47, No. 1, 46-60

Nguyen-Sy, L. (2006). *The theoretical modelling of circular shallow foundation for offshore wind turbines*. Ph.D. thesis, Oxford University

Nova, R. and Montrasio, L. (1991). Settlements of shallow foundations on sand. *Géotechnique* 41, No. 2, 243-256

Roscoe, K. H. and Schofield, A. N. (1956). The stability of a short pier foundations in sand. *British Welding Journal*. August, 343-354

Salciarini, D. and Tamagnini, C. (2009). A hypoplastic macroelement model for shallow foundations under monotonic and cyclic loads. *Acta Geotechnica* 4, No. 3, 163-176

Tamagnini, C., Salciarini, D. and Ragni, R. (2013). Implementation of a 6-dof hypoplastic macroelement in a finite element code. In *Proceeding of the International Conference on Computational Geomechanics (Comgeo III), Krakow*

Vaitkunaite, E., Ibsen, L. B., and Nielsen, B. N. (2014). New medium-scale laboratory testing of bucket foundation capacity in sand. In *Proceedings of the Twenty-fourth International Ocean and Polar Engineering Conference (ISOPE), Busan*

Villalobos, F. A. (2006). *Model testing of foundations for offshore wind turbines*. Ph.D. thesis, Oxford University

Villalobos, F. A., Byrne, B. W. and Houlsby, G. T. (2009). An experimental study of the drained capacity of suction caisson foundations under monotonic loading for offshore applications. *Soils and Foundations* 49, No. 3, 477-488

Wood, D. M. (2012). Macroelement modelling. In *Mechanical Behaviour of Soils under Environmentally Induced Cyclic Loads*, di Prisco C. and Wood D. M. (Eds), CISM, Udine

Zhang, Y., Cassidy, M. J., Bienen, B. (2014). A plasticity model for spudcan foundations in soft clay. *Canadian Geotechnical Journal* 51, 629-646

ISSN 1901-7278
DCE Technical Memorandum No. 48